Semantic Image Synthesis with Spatially-Adaptive Normalization

Taesung Park[1]* Ming-Yu Liu[2] Ting-Chun Wang[2] Jun-Yan Zhu[2,3]

[1]University of California, Berkeley [2]NVIDIA [3]Massachusetts Institute of Technology

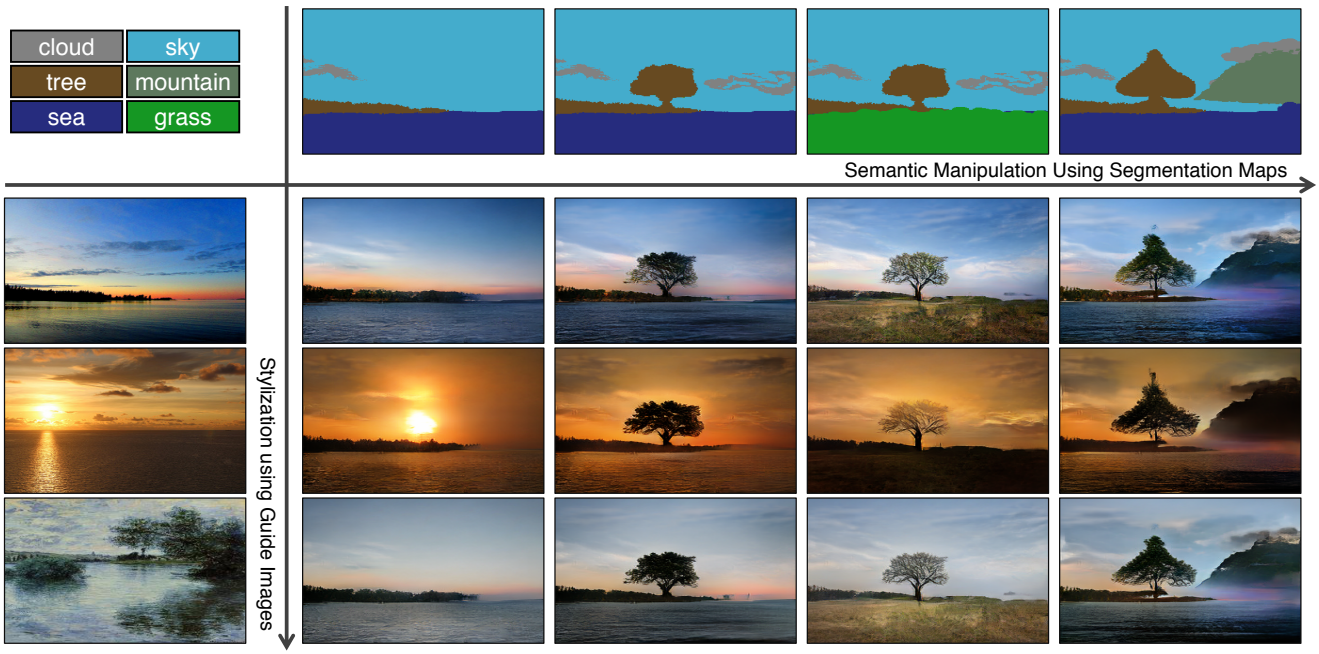

Figure 1: Our model generates high fidelity images that respect both semantic layout and style of the guide image. The semantics (e.g., existence of a tree) can be controlled using the label map in the top row. On the other hand, style of the image, namely the attributes that cannot be expressed from the label map, can be controlled using the guide images in leftmost column. Please see our video at https://NVlabs.github.io/SPADE for interactive photo manipulation.

Abstract

We propose spatially-adaptive normalization, a simple but effective layer for synthesizing photorealistic images given an input semantic layout. Previous methods directly feed the semantic layout as input to the network, which is then processed through stacks of convolution, normalization, and nonlinearity layers. We show that this is suboptimal because existing normalization layers tend to wash away semantic information. To address the issue, we propose using the input layout for modulating the activations in normalization layers through a spatially-adaptive, learned affine transformation. Experiments on several challenging datasets demonstrate the advantage of the proposed method compared to existing approaches, regarding both visual fidelity and alignment with input layouts. Finally, our model allows users to easily control the style and content of synthesis results as well as create multi-modal results. Code is available at https://github.com/NVlabs/SPADE

1. Introduction

Conditional image synthesis refers to the task of generating photorealistic images conditioning on some input data such as text, label, image, or segmentation mask. Earlier methods compute the output image by stitching patches from a database of images [3, 13]. Recent methods directly learn the mapping using neural networks [4, 7, 20, 39, 40, 45,

*Taesung Park contributed to the work during his NVIDIA internship.

Type	Normalization scheme
Unconditional	BN [19], IN [38], LN [2], WN [37], GN [41], LRN [24]
Conditional	Conditional BN [9, 10], AdaIN [17]
Conditional and spatially-adaptive	**Proposed**

Table 1: Normalization comparison. Existing unconditional- and conditional- normalizations use spatially invariant transform, so they cannot model local structure of the input segmentation mask.

46, 47]. The learning-based methods enjoy several advantages over the earlier approaches. They are faster and do not require an external database of images.

We are interested in a specific form of conditional image synthesis, which is converting a semantic segmentation mask to a photorealistic image. This form has a wide range of applications such as photo manipulation and content generation [7, 20, 40]. We will refer to this form as semantic image synthesis. In this paper, we show that the conventional semantic image synthesis network architecture [20, 40], which is built by stacking convolutional, normalization, and nonlinearity layers, is at best sub-optimal, because the normalization layers tend to wash away information in input semantic masks. To address the issue, we propose *spatially-adaptive normalization* layer, a simple but effective conditional normalization layer. Our new normalization layer uses the input semantic layout to modulate the activations through a spatially-adaptive, learned affine transformation, effectively propagating the semantic information throughout the network.

We conduct experiments on several challenging datasets including the COCO-Stuff [5, 26], the ADE20K [48], and the Cityscapes [8]. We show that with the help of our spatially-adaptive normalization layer, a small, compact network can synthesize significantly better results compared to several state-of-the-art methods. Additionally, an extensive ablation study demonstrates the effectiveness of the proposed normalization layer against several variants for the semantic image synthesis task. Finally, our method supports multi-modal generation and guided image synthesis, enabling controllable, diverse outputs as shown in Figure 1.

2. Related Work

Deep generative models can learn to sample images. Recent methods include generative adversarial networks (GANs) [12] and variational autoencoder (VAE) [22]. Our work is built on GANs but aims for the conditional image synthesis task. The GANs consist of a generator and a discriminator where goal of the generator is to produce realistic images so that the discriminator cannot tell the synthesized images apart from real ones.

Conditional image synthesis exists in many forms that differ in input data type. For example, when the input data are single class labels, we have a class-conditional image synthesis model [4, 29, 31, 33]. When the input data are text, we have text-to-image models [16, 36, 43, 46]. Another popular form is image-to-image translation [18, 20, 23, 27, 49, 50], where both input and output are images. The conditional image synthesis models can be trained with or without input-output training pairs. We focus on converting segmentation masks to photorealistic images in the paired setting. We show that by using the proposed spatially-adaptive normalization layer, our compact network can achieve better results compared to leading methods.

Normalization layers have been an important component in modern deep networks and can be found in various classifier designs, including the Local Response Normalization (LRN) in the AlexNet [24] and Batch Normalization (BN) in the Inception-v2 network [19]. Other popular normalization layers include the Instance Normalization (IN) [38], Layer Normalization (LN) [2], Group Normalization [41], and Weight Normalization (WN) [37]. We label these normalization layers as unconditional as they do not depend on external data in contrast to the conditional normalization layers discussed below.

Conditional normalization layers include representatives such as the Conditional Batch Normalization (Conditional BN) [10] and Adaptive Instance Normalization (AdaIN) [17]. Both were first used in the style transfer task and later adopted in various vision tasks [9, 18, 29, 31, 34, 45]. Different from the earlier normalization techniques, conditional normalization layers require external data and generally operate as follows. First, layer activations are normalized to zero mean and unit deviation. Then the normalized activations are *denormalized* to modulate the activation by a learned transformation whose parameters are inferred from external data. For style transfer tasks [10, 17], the affine parameters are used to control the global style of the output, and hence are uniform across spatial coordinates. This characterizes the major difference in our proposed normalization layer, which applies a spatially-varying affine transformation. We compare the proposed spatially-adaptive normalization to the other normalizations in Table 1.

3. Semantic Image Synthesis

Let $\mathbf{m} \in \mathbb{L}^{H \times W}$ be a semantic segmentation mask where $\mathbb{L}$ is a set of integers denoting the semantic labels, and H and W are the image height and width. Each entry in $\mathbf{m}$ denotes the semantic label of a pixel. The semantic image synthesis problem is about learning a mapping function g, modeled via a deep convolutional neural network, that can convert the segmentation mask $\mathbf{m}$ to a photorealistic image $\mathbf{x} = g(\mathbf{m})$.

Spatially-adaptive denormalization. Let $\mathbf{h}^i$ denotes the

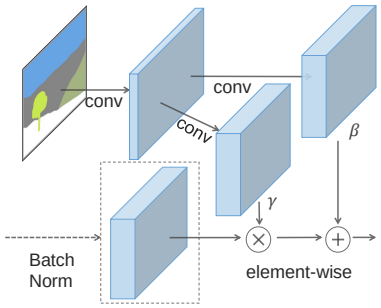

Figure 2: In SPADE, the mask is first projected onto an embedding space, and then convolved to produce the modulation parameters $\boldsymbol{\gamma}$ and $\boldsymbol{\beta}$. Unlike prior conditional normalization methods, $\boldsymbol{\gamma}$ and $\boldsymbol{\beta}$ are not vectors, but tensors with spatial dimensions. The produced $\boldsymbol{\gamma}$ and $\boldsymbol{\beta}$ are multiplied and added to the normalized activation element-wise.

activations of the i-th layer of a deep convolutional network computed as processing a batch of N samples. Let C^i be the number of channels in the layer. Let H^i and W^i be the height and width of the activation map in the layer. We propose a new conditional normalization method called SPatially-Adaptive (DE)normalization[1] (SPADE). Similar to Batch Normalization [19], the activation is normalized in the channel-wise manner, and then modulated with learned scale and bias. The activation value at site $(n \in N, c \in C^i, y \in H^i, x \in W^i)$ is given by

$$\gamma^i_{c,y,x}(\mathbf{m})\frac{h^i_{n,c,y,x} - \mu^i_c}{\sigma^i_c} + \beta^i_{c,y,x}(\mathbf{m}) \tag{1}$$

where $h^i_{n,c,y,x}$ is the activation at the site before normalization, μ^i_c and σ^i_c are the mean and standard deviation of the activation in channel c. Note that computation of μ^i_c and σ^i_c is same as that in the batch normalization method [19]:

$$\mu^i_c = \frac{1}{H^i W^i}\sum_{n,y,x} h^i_{n,c,y,x} \tag{2}$$

$$\sigma^i_c = \sqrt{\frac{1}{H^i W^i}\sum_{n,y,x}(h^i_{n,c,y,x})^2 - (\mu^i_c)^2}. \tag{3}$$

The variables $\gamma^i_{c,y,x}(\mathbf{m})$ and $\beta^i_{c,y,x}(\mathbf{m})$ in (1) are the learned modulation parameters of the normalization layer. In contrast to batchnorm [19], they depend on the input segmentation mask and vary with respect to the location (y, x). We use the symbol $\gamma^i_{c,y,x}$ and $\beta^i_{c,y,x}$ to denote the function mappings that convert the input segmentation mask $\mathbf{m}$ to the scaling and bias values at the site (c, y, x) in the activation map of the i-th layer of the deep network. In this paper, we implement the function mappings $\gamma^i_{c,y,x}$ and $\beta^i_{c,y,x}$ using a simple two-layer convolutional network. The details of the network design are given in the supplementary material.

In fact, SPADE is related to, and is a generalization of several existing normalization layers. First, replacing the segmentation mask $\mathbf{m}$ with the image class label and making the modulation parameters spatially-invariant (i.e., $\gamma^i_{c,y_1,x_1} \equiv \gamma^i_{c,y_2,x_2}$ and $\beta^i_{c,y_1,x_1} \equiv \beta^i_{c,y_2,x_2}$ for any $y_1, y_2 \in \{1, 2, ..., H^i\}$ and $x_1, x_2 \in \{1, 2, ..., W^i\}$), we arrive at the form of conditional batch normalization layer [10]. Indeed, for any spatially-invariant conditional data, our method reduces to Conditional BN. Similarly, we can arrive at AdaIN [17] by replacing the segmentation mask with another image, making the modulation parameters spatially-invariant and setting $N = 1$. As the modulation parameters are adaptive to the input segmentation mask, the proposed SPADE is better suited for semantic image synthesis. Figure 2 illustrates the SPADE design.

SPADE generator. With SPADE, there is no need to feed the segmentation map to the first layer of the generator, since the learned modulation parameters provide enough signal about the label layout. Therefore, we can discard encoder part of the generator, which is commonly used in recent architectures such as pix2pixHD [40]. Doing so results in a more lightweight network. Furthermore, similarly to existing class-conditional generators [29, 31, 45], the new generator can take a random vector as input, which enables a simple and natural way for multi-modal synthesis.

Figure 3 illustrates our generator architecture, which employs several ResNet blocks [14] with upsampling layers. The modulation parameters of all the normalization layers are learned using SPADE. Since each residual block operates in a different scale, SPADE downsamples the semantic mask to match the spatial resolution. The input to the first layer of the generator can be a random noise sampled from unit Gaussian, or a downsampled segmentation map. These two produce very similar results as shown in Table 5.

We train the generator with the same multi-scale discriminator and loss function used in pix2pixHD except that we replace the least squared loss term [28] with the hinge loss term [25, 30, 45]. We test several ResNet-based discriminators used in recent unconditional GANs [1, 29, 31] but find them render a similar performance at the cost of a higher GPU memory requirement. Adding the SPADE to the discriminator also yields a similar performance. For the loss function, we observe that removing any loss term in the pix2pixHD loss function will worsen the results.

Why does SPADE work better? A short answer is that it can better preserve semantic information against common normalization layers. Specifically, while normalization layers such as the IN [38] are essential pieces in almost all the state-of-the-art conditional image synthesis models [40], they tend to wash away semantic information when applied to uniform or flat segmentation masks.

[1] Conditional normalization methods [10, 17] use inputs for denormalizing the normalized activations; i.e., the denormalization part is conditional.

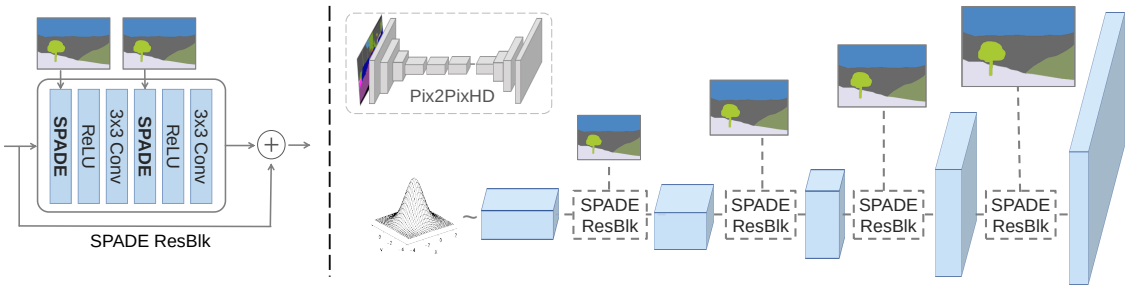

Figure 3: In SPADE Generator, the signal from the segmentation mask is inputted at each normalization layer to modulate the layer activations. The generator contains a series of SPADE residual blocks with upsampling. Our architecture achieves superior performance with smaller number of parameters than the leading semantic segmentation network.

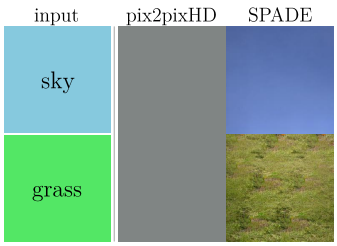

Figure 4: SPADE and pix2pixHD given uniform segmentation map. While SPADE produces plausible texture for each class, pix2pixHD produces identical outputs due to the loss of the semantic information after the normalization layer.

Let us consider a simple module that first applies convolution to a segmentation mask and then normalization. Furthermore, let us assume that a segmentation mask with a single label is given as input to the module (e.g., all the pixels have the same label such as sky or grass). Under this setting, the convolution outputs are again uniform with different labels having different uniform values. Now after we apply IN to the output, the normalized activation will become all zeros no matter what the input semantic label is given. Therefore, semantic information is totally lost. This limitation applies to a wide range of generator architectures, including pix2pixHD and its variant that concatenates the semantic mask at all intermediate layers, as long as a network applies convolution and then normalization to the semantic mask. In Figure 4, we empirically show this is precisely the case for the pix2pixHD. Because a segmentation mask consists of a few uniform regions in general, they suffer from information loss when applying normalization.

In contrast, the segmentation mask in the SPADE Generator is fed through a spatially adaptive modulation module *without* any normalization layer. Only feature activations from the previous layer are normalized. Hence, the SPADE generator can better preserve semantic information. Hence, it enjoys the benefit of normalization layers without losing the semantic input information.

Multi-modal synthesis. By using random vector at input of the generator, our architecture provides a simple way for multi-modal synthesis. Namely, one can attach an encoder e that processes a real image into a random vector, which will be then fed to the generator. The encoder and generator form a variational autoencoder [22], in which the encoder tries to capture the style of the image, while the generator combines the encoded style and the segmentation mask information via SPADE to reconstruct the original image. The encoder also serves as a style guidance network at test time to capture the styles of target images, as used in Figure 1. For training, we add a KL-Divergence loss term [22].

4. Experiments

Implementation details. We apply the Spectral Norm [30] to all the layers in both the generator and discriminator. We use the Two Time-scale Update Rule [15] for training where the learning rates for the generator and discriminator are set to 0.0001 and 0.0004, respectively. We use the ADAM optimizer [21] and set $\beta_1 = 0$, $\beta_2 = 0.999$. All the experiments are conducted on an NVIDIA DGX1 machine with 8 V100 GPUs. We use synchronized mean and variance computation, i.e., these statistics are collected from all the GPUs.

Datasets. We conduct experiments using several datasets.

- *COCO-Stuff* [5] is derived from the COCO dataset [26]. It has 118000 training images and 5000 validation images captured from diverse scenes. It has 182 semantic classes. Due to large diversity, existing image synthesis models perform poorly on this dataset.
- *ADE20K* [48] consists of 20210 training and 2000 validation images. Similarly to COCO, the dataset contains diverse scenes with 150 semantic classes.
- *ADE20K-outdoor* is a subset of the ADE20K dataset that only contains outdoor scenes.
- *Cityscapes* dataset [8] contains street scene images in German cities. The training and validation set sizes are 3000 and 500, respectively. Recent work has achieved photorealistic semantic image synthesis results [35, 39] on the Cityscapes dataset.
- *Flickr Landscapes.* We collect 41000 photos from Flickr and use 1000 samples for the validation set. Instead of

Figure 5: Visual comparison of semantic image synthesis results on the COCO-Stuff dataset.

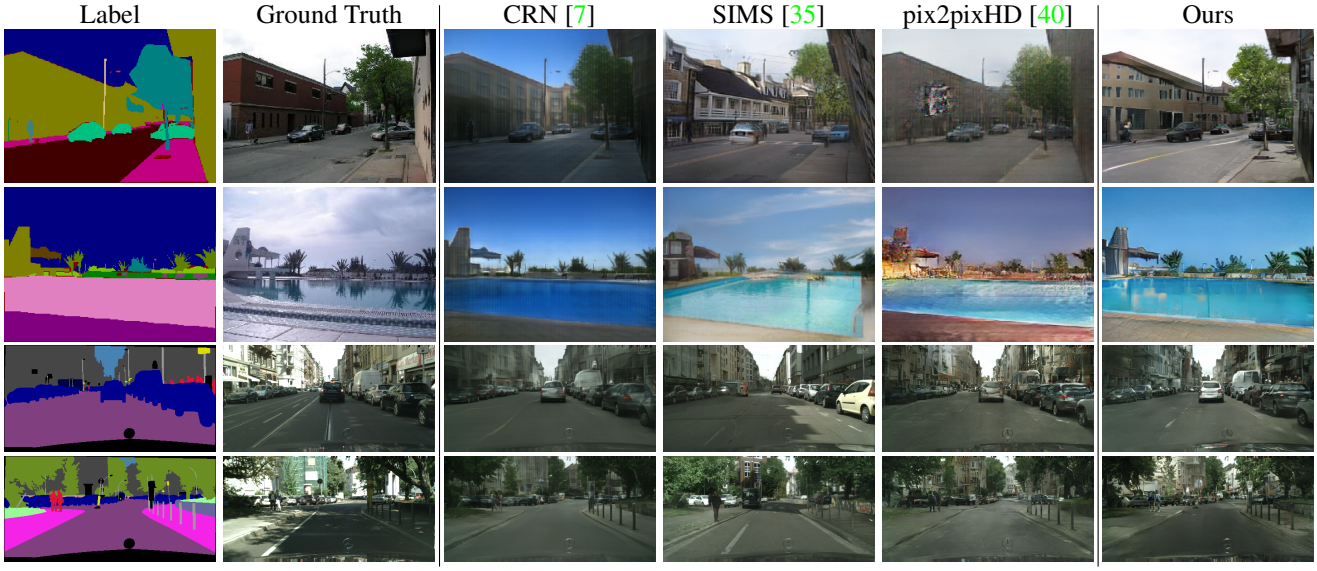

Figure 6: Visual comparison of semantic image synthesis results on the ADE20K outdoor and Cityscapes datasets.

	COCO-Stuff			ADE20K			ADE20K-outdoor			Cityscapes		
Method	mIoU	accu	FID	mIoU	accu	FID	mIoU	accu	FID	mIoU	accu	FID
CRN [7]	23.7	40.4	70.4	22.4	68.8	73.3	16.5	68.6	99.0	52.4	77.1	104.7
SIMS [35]	N/A	N/A	N/A	N/A	N/A	N/A	13.1	74.7	67.7	47.2	75.5	**49.7**
pix2pixHD [40]	14.6	45.8	111.5	20.3	69.2	81.8	17.4	71.6	97.8	58.3	81.4	95.0
Ours	**37.4**	**67.9**	**22.6**	**38.5**	**79.9**	**33.9**	**30.8**	**82.9**	**63.3**	**62.3**	**81.9**	71.8

Table 2: Our method outperforms current leading methods in semantic segmentation scores (mean IoU and overall pixel accuracy) and FID [15] on all the benchmark datasets. For mIoU and pixel accuracy, higher is better. For FID, lower is better.

manually annotation, we use a pretrained DeepLabV2 [6] model to compute the input segmentation masks.

We train the competing semantic image synthesis methods using the training set and evaluate their performance on the validation set for each dataset.

Performance metrics. We adopt the evaluation protocol from the previous works [7, 40]. Specifically, we perform semantic segmentation on the synthesized images and compare how well the predicted segmentation mask matches the input. This is based on the intuition that if the output images are realistic then a well-trained semantic segmentation model should be able to predict the ground truth label. For measuring the segmentation accuracy, we use the mean Intersection-over-Union (mIoU) and pixel accuracy (accu) metrics. For the segmentation network, we use DeepLabV2 [6, 32] for COCO-Stuff, UperNet101 [42] for ADE20K, and DRN-D-105 [44] for Cityscapes. In addition to segmentation accuracy, we use the Fréchet Inception Distance (FID) [15] to measure the similarity between the distributions of the synthesized and ground truth images.

Baselines. We compare our method with three leading semantic image synthesis models: the Cascaded Refinement Network model (CRN) [7], the Semi-Parametric Image Synthesis model (SIMS) [35], and the pix2pixHD [40]

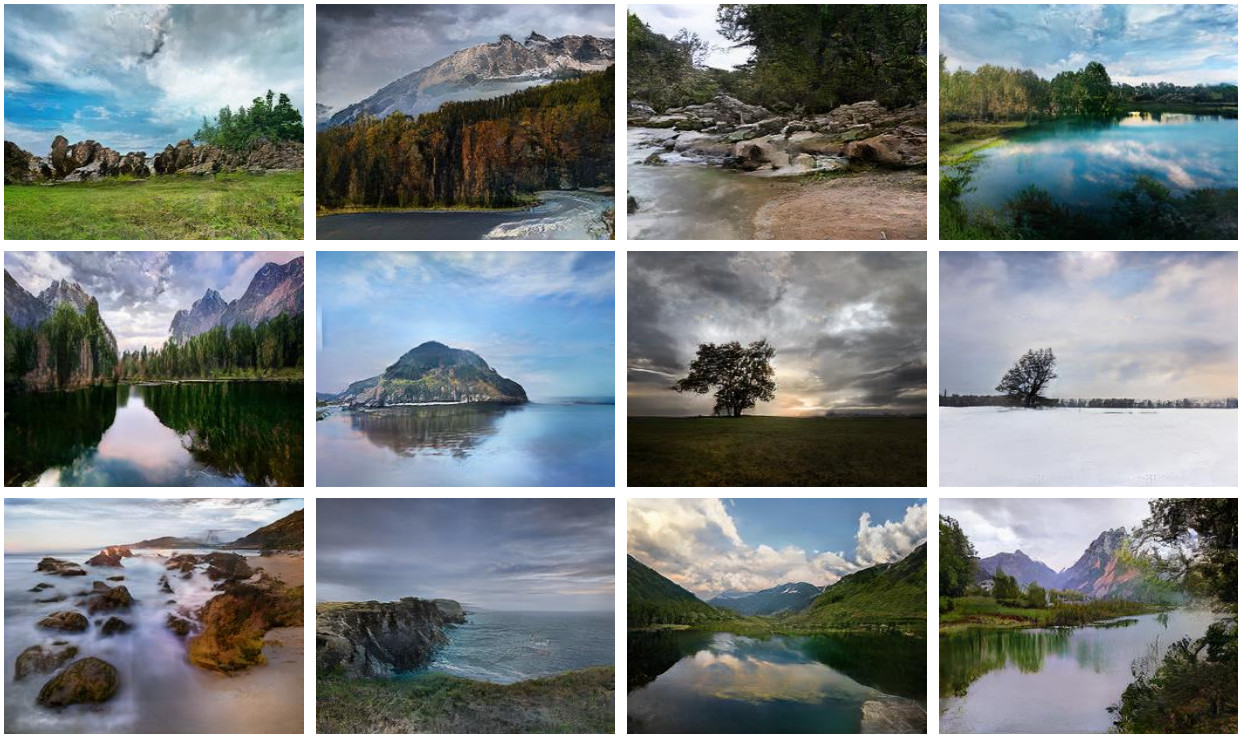

Figure 7: Semantic image synthesis results on the Flickr Landscapes dataset.

model. CRN uses a deep network that repeatedly refines the output from low to high resolution, while the SIMS takes a semi-parametric approach that collages real patches from the training set and refines the boundaries. Both the CRN and SIMS are mainly trained using image reconstruction loss. pix2pixHD is the current state-of-the-art GAN-based conditional image synthesis framework. For a fair comparison, we train the CRN and pix2pixHD models using the implementations provided by the authors. As synthesizing an image using the SIMS model requires many queries to the training dataset, it is computationally prohibitive for a large dataset such as COCO-stuff and the full ADE20K. Therefore, we use the result images provided by the authors whenever possible.

Main results. As shown in Table 2, our method outperforms the current state-of-the-art methods by a large margin in all the datasets. For COCO-Stuff, our method achieves a mIoU score of 35.2, which is about 1.5 times better than the previous leading method. Our FID is also 2.2 times better than the previous leading method. We note that the SIMS model produces a lower FID score but has poor segmentation performances on the Cityscapes dataset. This is because the SIMS synthesizes an image by first stitching image patches from the training dataset. As using the real image patches, the resulting image distribution can match the real image distribution more easily. However, because there is no guarantee that a perfect query (e.g., a person in a particular pose) exists in the dataset, it tends to copy objects with mismatched segments.

Dataset	Ours vs. CRN	Ours vs. pix2pixHD	Ours vs. SIMS
COCO-Stuff	79.76	86.64	N/A
ADE20K	76.66	83.74	N/A
ADE20K-outdoor	66.04	79.34	85.70
Cityscapes	63.60	53.64	51.52

Table 3: User preference score. The numbers indicate the percentage of users who favor the results of the proposed method over the competing method.

Visual results. In Figures 5 and 6, we provide a visual comparison of the competing methods. We found that our method produces much better visual quality with much fewer artifacts, especially for diverse scenes in the COCO-Stuff and ADE20K dataset. When the training dataset size is small, the SIMS model also renders images with good visual quality. However, the depicted content often deviates from the input segmentation mask (e.g., the shape of the swimming pool in the second row of Figure 6).

In Figures 7 and 8, we visualize synthesis results from the Flickr Landscape and COCO-Stuff datasets. The proposed method can generate diverse scenes with high image fidelity. More results are in the supplementary materials.

Human evaluation. We use Amazon Mechanical Turk to compare the perceived visual fidelity of our method against

Figure 8: Semantic image synthesis results on COCO-Stuff.

Method	#param	COCO	ADE20K	Cityscapes
Ours	96M	**35.2**	38.5	62.3
Ours (fewer params)	61M	**35.2**	38.0	**62.5**
Concat w/o SPADE	79M	31.9	33.6	61.1
P2P++ w/ SPADE	237M	34.4	**39.0**	62.2
P2P++ w/ Concat	195M	32.9	38.9	57.1
P2P++	183M	32.7	38.3	58.8
P2P++ (fewer params)	103M	31.6	37.3	57.6
pix2pixHD [40]	183M	14.6	20.3	58.3

Table 4: mIoU scores of variants of our model and a strong baseline (P2P++) with and without SPADE. Adding SPADE boosts performance in both architectures, while simple concatenation method fails to do so. Moreover, our model outperforms all others with smaller number of parameters.

existing leading approaches. Specifically, we give the workers an input segmentation mask and two synthesis outputs from different methods and ask them to choose the output image that looks more like a corresponding image of the segmentation mask. The workers are given unlimited time to make the selection. For each comparison, we randomly generate 500 questions for each dataset, and each question is answered by 5 different workers. For quality control, a worker must have a lifetime task approval rate greater than 98% to be able to participate in the evaluation.

Table 3 shows the evaluation results. We find that the users have a strong preference on the results generated by the proposed method on all the datasets, especially on the challenging COCO-Stuff and ADE20K datasets. For the Cityscapes, all the competing methods achieve high image fidelity. Still, the users still favor our results.

Method	COCO	ADE20K	Cityscapes
segmap input	35.2	38.5	62.3
random input	35.3	38.3	61.6
kernelsize 5x5	35.0	39.3	61.8
kernelsize 3x3	35.2	38.5	62.3
kernelsize 1x1	32.7	35.9	59.9
#params 141M	35.3	38.3	62.5
#params 96M	35.2	38.5	62.3
#params 61M	35.2	38.0	62.5
Sync Batch norm	35.0	39.3	61.8
Batch Norm	33.7	37.9	61.8
Instance Norm	33.9	37.4	58.7

Table 5: The SPADE generator works on many different configurations. We change the input of the generator network, the convolutional kernel size acting on the segmentation map, the capacity of the network, and the parameter-free normalization method. The settings used in the paper are boldfaced.

Impact of SPADE. To verify effectiveness of SPADE, we introduce a strong baseline called P2P++, which combines all the techniques we find useful for enhancing the performance except SPADE to the architecture of pix2pixHD. We also train models that receive segmentation mask input at all the intermediate layers via concatenation (P2P++ w/ Concat) in the channel direction. Finally, the model that combines the strong baseline with SPADE is denoted as (P2P++ w/ SPADE). Additionally, we compare models under different capacity by using a different number of convolutional filters in the generator.

As shown in Table 4 the architectures with the proposed SPADE consistently outperforms its counterparts. We also

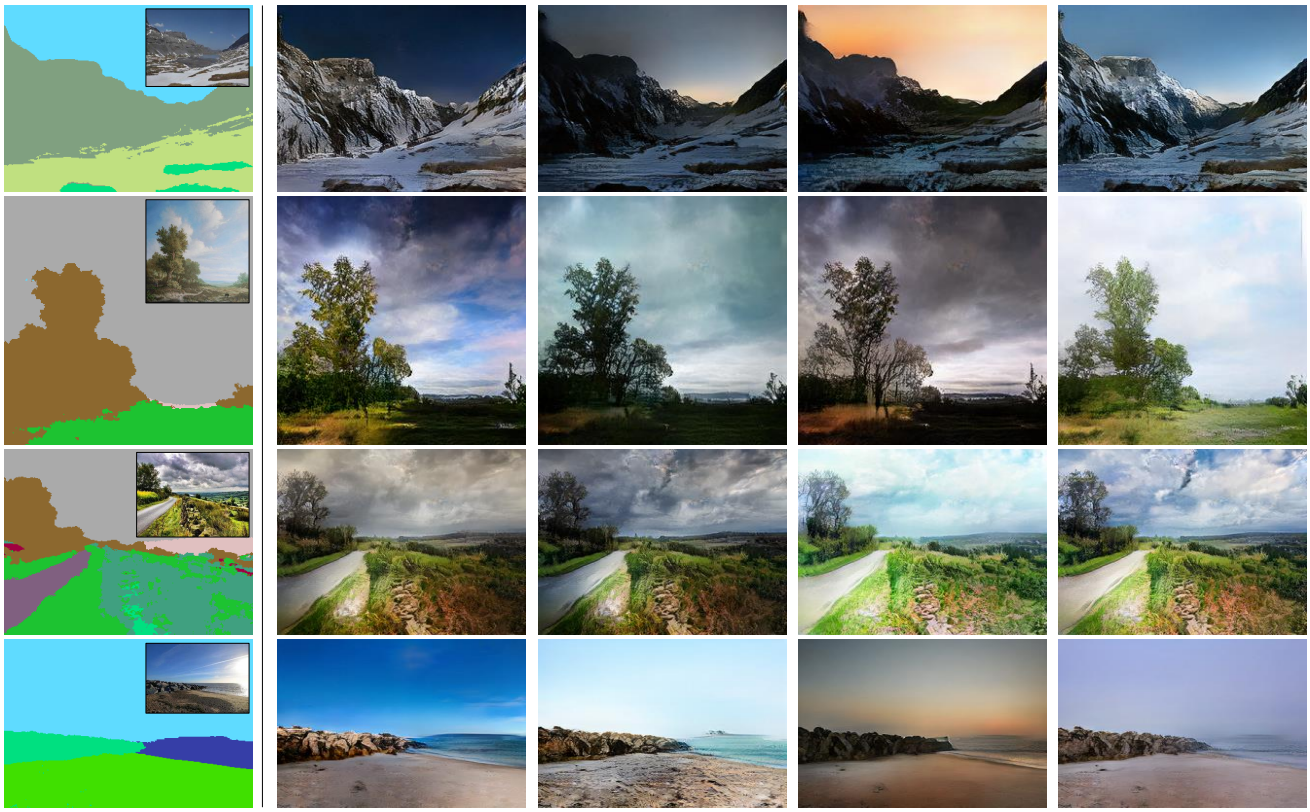

Figure 9: Our model attains multimodal synthesis capability when trained with the image encoder. During deployment, by using different random noise, our model synthesizes outputs with diverse appearances but all having the same semantic layouts depicted in the input mask. For reference, the ground truth image is shown inside the input segmentation mask.

find that providing decoders the segmentation masks via SPADE leads to consistently better performance than those via concatenation. Furthermore, the SPADE generator achieves much better performance than the strong baselines by using a smaller number of parameters.

Variations of SPADE generator. We report performance of variations of our generator. First, we compare using random noise to using downsampled segmentation maps as the input of the generator network to study the role of randomness in the generator network. We find that both render similar performance, and conclude that the modulation by SPADE alone provides sufficient signal about the input segmentation mask. Second, we vary the type of parameter-free normalization prior to the application of the modulation parameters of SPADE. We observe that SPADE works reliably across different normalization methods. Next, we vary the convolutional kernel size acting on the label map, and observe that kernel size of 1x1 hurts performance, likely because it prohibits utilizing the context of the label. Lastly, we change the capacity of the generator network simply by changing the number of convolutional filters. We present more variations and ablations in the supplementary materials for more detailed investigation.

Multi-modal synthesis. In Figure 9, we show the multimodal image synthesis results on the Flickr Landscape dataset. For the same input segmentation mask, we sample different noise inputs for achieving diverse outputs. More results are in the supplemental materials.

Semantic manipulation and guided image synthesis. In Figure 1, we show an application where a user draws different segmentation mask and our model render the corresponding landscape images. Moreover, our model allows users to choose an external style image to control the global appearances of the output image. This is achieved by replacing the input noise with the image embedding of the style image computed by the image encoder e.

5. Conclusion

We propose the spatially-adaptive normalization, which utilizes the input semantic layout while performing the affine transformation in the normalization layers. We show that using the proposed normalization leads to the first semantic image synthesis generator that can produce photorealistic outputs for diverse scenes including indoor, outdoor, landscape, and street scenes. We further show its application for multi-modal synthesis and guided image synthesis.

References

[1] M. Arjovsky, S. Chintala, and L. Bottou. Wasserstein generative adversarial networks. In *International Conference on Machine Learning (ICML)*, 2017. 3

[2] J. L. Ba, J. R. Kiros, and G. E. Hinton. Layer normalization. *arXiv preprint arXiv:1607.06450*, 2016. 2

[3] C. Barnes, E. Shechtman, A. Finkelstein, and D. B. Goldman. Patchmatch: A randomized correspondence algorithm for structural image editing. In *ACM SIGGRAPH*, 2009. 1

[4] A. Brock, J. Donahue, and K. Simonyan. Large scale gan training for high fidelity natural image synthesis. In *International Conference on Learning Representations (ICLR)*, 2019. 1, 2

[5] H. Caesar, J. Uijlings, and V. Ferrari. Coco-stuff: Thing and stuff classes in context. In *IEEE Conference on Computer Vision and Pattern Recognition (CVPR)*, 2018. 2, 4

[6] L.-C. Chen, G. Papandreou, I. Kokkinos, K. Murphy, and A. L. Yuille. Deeplab: Semantic image segmentation with deep convolutional nets, atrous convolution, and fully connected crfs. *IEEE transactions on pattern analysis and machine intelligence*, 40(4):834–848, 2018. 5

[7] Q. Chen and V. Koltun. Photographic image synthesis with cascaded refinement networks. In *IEEE International Conference on Computer Vision (ICCV)*, 2017. 1, 2, 5

[8] M. Cordts, M. Omran, S. Ramos, T. Rehfeld, M. Enzweiler, R. Benenson, U. Franke, S. Roth, and B. Schiele. The cityscapes dataset for semantic urban scene understanding. In *IEEE Conference on Computer Vision and Pattern Recognition (CVPR)*, 2016. 2, 4

[9] H. De Vries, F. Strub, J. Mary, H. Larochelle, O. Pietquin, and A. C. Courville. Modulating early visual processing by language. In *Advances in Neural Information Processing Systems (NIPS)*, 2017. 2

[10] V. Dumoulin, J. Shlens, and M. Kudlur. A learned representation for artistic style. In *International Conference on Learning Representations (ICLR)*, 2016. 2, 3

[11] X. Glorot and Y. Bengio. Understanding the difficulty of training deep feedforward neural networks. In *Proceedings of the thirteenth international conference on artificial intelligence and statistics*, pages 249–256, 2010.

[12] I. Goodfellow, J. Pouget-Abadie, M. Mirza, B. Xu, D. Warde-Farley, S. Ozair, A. Courville, and Y. Bengio. Generative adversarial nets. In *Advances in Neural Information Processing Systems (NIPS)*, 2014. 2

[13] J. Hays and A. A. Efros. Scene completion using millions of photographs. In *ACM SIGGRAPH*, 2007. 1

[14] K. He, X. Zhang, S. Ren, and J. Sun. Deep residual learning for image recognition. In *IEEE Conference on Computer Vision and Pattern Recognition (CVPR)*, 2016. 3

[15] M. Heusel, H. Ramsauer, T. Unterthiner, B. Nessler, and S. Hochreiter. GANs trained by a two time-scale update rule converge to a local Nash equilibrium. In *Advances in Neural Information Processing Systems (NIPS)*, 2017. 4, 5

[16] S. Hong, D. Yang, J. Choi, and H. Lee. Inferring semantic layout for hierarchical text-to-image synthesis. In *IEEE Conference on Computer Vision and Pattern Recognition (CVPR)*, 2018. 2

[17] X. Huang and S. Belongie. Arbitrary style transfer in real-time with adaptive instance normalization. In *IEEE International Conference on Computer Vision (ICCV)*, 2017. 2, 3

[18] X. Huang, M.-Y. Liu, S. Belongie, and J. Kautz. Multimodal unsupervised image-to-image translation. *European Conference on Computer Vision (ECCV)*, 2018. 2

[19] S. Ioffe and C. Szegedy. Batch normalization: Accelerating deep network training by reducing internal covariate shift. In *International Conference on Machine Learning (ICML)*, 2015. 2, 3

[20] P. Isola, J.-Y. Zhu, T. Zhou, and A. A. Efros. Image-to-image translation with conditional adversarial networks. In *IEEE Conference on Computer Vision and Pattern Recognition (CVPR)*, 2017. 1, 2

[21] D. P. Kingma and J. Ba. Adam: A method for stochastic optimization. In *International Conference on Learning Representations (ICLR)*, 2015. 4

[22] D. P. Kingma and M. Welling. Auto-encoding variational bayes. In *International Conference on Learning Representations (ICLR)*, 2014. 2, 4

[23] A. Kolliopoulos, J. M. Wang, and A. Hertzmann. Segmentation-based 3d artistic rendering. In *Rendering Techniques*, pages 361–370, 2006. 2

[24] A. Krizhevsky, I. Sutskever, and G. E. Hinton. Imagenet classification with deep convolutional neural networks. In *Advances in Neural Information Processing Systems (NIPS)*, 2012. 2

[25] J. H. Lim and J. C. Ye. Geometric gan. *arXiv preprint arXiv:1705.02894*, 2017. 3

[26] T.-Y. Lin, M. Maire, S. Belongie, J. Hays, P. Perona, D. Ramanan, P. Dollár, and C. L. Zitnick. Microsoft coco: Common objects in context. In *European Conference on Computer Vision (ECCV)*, 2014. 2, 4

[27] M.-Y. Liu, T. Breuel, and J. Kautz. Unsupervised image-to-image translation networks. In *Advances in Neural Information Processing Systems (NIPS)*, 2017. 2

[28] X. Mao, Q. Li, H. Xie, Y. R. Lau, Z. Wang, and S. P. Smolley. Least squares generative adversarial networks. In *IEEE International Conference on Computer Vision (ICCV)*, 2017. 3

[29] L. Mescheder, A. Geiger, and S. Nowozin. Which training methods for gans do actually converge? In *International Conference on Machine Learning (ICML)*, 2018. 2, 3

[30] T. Miyato, T. Kataoka, M. Koyama, and Y. Yoshida. Spectral normalization for generative adversarial networks. In *International Conference on Learning Representations (ICLR)*, 2018. 3, 4

[31] T. Miyato and M. Koyama. cGANs with projection discriminator. In *International Conference on Learning Representations (ICLR)*, 2018. 2, 3

[32] K. Nakashima. Deeplab-pytorch. https://github.com/kazuto1011/deeplab-pytorch, 2018. 5

[33] A. Odena, C. Olah, and J. Shlens. Conditional image synthesis with auxiliary classifier GANs. In *International Conference on Machine Learning (ICML)*, 2017. 2

[34] E. Perez, H. De Vries, F. Strub, V. Dumoulin, and A. Courville. Learning visual reasoning without strong priors. In *International Conference on Machine Learning (ICML)*, 2017. 2

[35] X. Qi, Q. Chen, J. Jia, and V. Koltun. Semi-parametric image synthesis. In *IEEE Conference on Computer Vision and Pattern Recognition (CVPR)*, 2018. 4, 5

[36] S. Reed, Z. Akata, X. Yan, L. Logeswaran, B. Schiele, and H. Lee. Generative adversarial text to image synthesis. In *International Conference on Machine Learning (ICML)*, 2016. 2

[37] T. Salimans and D. P. Kingma. Weight normalization: A simple reparameterization to accelerate training of deep neural networks. In *Advances in Neural Information Processing Systems (NIPS)*, 2016. 2

[38] D. Ulyanov, A. Vedaldi, and V. Lempitsky. Instance normalization: The missing ingredient for fast stylization. arxiv 2016. *arXiv preprint arXiv:1607.08022*, 2016. 2, 3

[39] T.-C. Wang, M.-Y. Liu, J.-Y. Zhu, G. Liu, A. Tao, J. Kautz, and B. Catanzaro. Video-to-video synthesis. In *Advances in Neural Information Processing Systems (NIPS)*, 2018. 1, 4

[40] T.-C. Wang, M.-Y. Liu, J.-Y. Zhu, A. Tao, J. Kautz, and B. Catanzaro. High-resolution image synthesis and semantic manipulation with conditional gans. In *IEEE Conference on Computer Vision and Pattern Recognition (CVPR)*, 2018. 1, 2, 3, 5, 7

[41] Y. Wu and K. He. Group normalization. In *European Conference on Computer Vision (ECCV)*, 2018. 2

[42] T. Xiao, Y. Liu, B. Zhou, Y. Jiang, and J. Sun. Unified perceptual parsing for scene understanding. In *European Conference on Computer Vision*. Springer, 2018. 5

[43] T. Xu, P. Zhang, Q. Huang, H. Zhang, Z. Gan, X. Huang, and X. He. Attngan: Fine-grained text to image generation with attentional generative adversarial networks. In *IEEE Conference on Computer Vision and Pattern Recognition (CVPR)*, 2018. 2

[44] F. Yu, V. Koltun, and T. A. Funkhouser. Dilated residual networks. In *CVPR*, 2017. 5

[45] H. Zhang, I. Goodfellow, D. Metaxas, and A. Odena. Self-attention generative adversarial networks. *arXiv preprint arXiv:1805.08318*, 2018. 1, 2, 3

[46] H. Zhang, T. Xu, H. Li, S. Zhang, X. Huang, X. Wang, and D. Metaxas. Stackgan: Text to photo-realistic image synthesis with stacked generative adversarial networks. In *IEEE International Conference on Computer Vision (ICCV)*, 2017. 1, 2

[47] H. Zhang, T. Xu, H. Li, S. Zhang, X. Wang, X. Huang, and D. Metaxas. Stackgan++: Realistic image synthesis with stacked generative adversarial networks. *IEEE Transactions on Pattern Analysis and Machine Intelligence (TPAMI)*, 2018. 1

[48] B. Zhou, H. Zhao, X. Puig, S. Fidler, A. Barriuso, and A. Torralba. Scene parsing through ade20k dataset. In *IEEE Conference on Computer Vision and Pattern Recognition (CVPR)*, 2017. 2, 4

[49] J.-Y. Zhu, T. Park, P. Isola, and A. A. Efros. Unpaired image-to-image translation using cycle-consistent adversarial networks. In *IEEE International Conference on Computer Vision (ICCV)*, 2017. 2

[50] J.-Y. Zhu, R. Zhang, D. Pathak, T. Darrell, A. A. Efros, O. Wang, and E. Shechtman. Toward multimodal image-to-image translation. In *Advances in Neural Information Processing Systems (NIPS)*, 2017. 2